Int. J. Environ. Res., 10(2):341-356, Spring 2016
ISSN: 1735-6865

Spatiotemporal Modeling of Net Primary Productivity of Eastern Mediterranean Biomes Under Different Regional Climate Change Scenarios

Donmez, C.[1*] , Berberoglu, S.[1], Cilek, A.[1], Evrendilek, F.[2]

[1] Department of Landscape Architecture, University of Cukurova, Adana 01330, Turkey

[2] Department of Environmental Engineering, University of Abant Izzet Baysal, Bolu, 14280, Turkey

Received 30 Nov. 2015; Revised 25 Feb. 2016; Accepted 29 Feb. 2016

ABSTRACT:The present study modeled how future terrestrial net primary productivity (NPP) changes spatiotemporally for the eastern Mediterranean biomes of Turkey using Carnegie Ames Stanford Approach (CASA) model, Moderate Resolution Imaging Spectroradiometer (MODIS) data, the four regional climate change scenarios (RCP 2.6, RCP 4.5, RCP 6.0 and RCP 8.5), and such ancillary data as percent tree cover, land use/cover map, soil texture, and normalized difference vegetation index (NDVI). A mean decrease occurred by 3.2% in the present (2000-2010) mean annual NPP of the most productive biome-deciduous broadleaf forest-in response to the average increases by 5 °C in maximum temperature, by 2 °C in minimum temperature, by 276 mm in maximum rainfall, and the average decrease by 69 mm in minimum rainfall among the RCPs for the future (2070-2100) period. The maximum annual NPP increases occurred by 4.4% for evergreen needle leaf forest, by 3.9% for grassland, 3.4% for cropland, 2.2% for mixed forest, and 1.1% for shrubland in response to RCP 8.5. Deciduous broadleaf forest NPP appeared to be more vulnerable than the other biomes to the decreased rainfall and the increased air temperature of the water-limited growing season projected by the RCPs. Increasing winter and spring temperatures appeared to benefit the earlier spring green-up of grasses, evergreen needle leaf trees, crops, and shrubs. Our results suggest that a shift from deciduous broadleaf forest toward conifer forest may become more widespread, in particular, in the southern, low-altitude areas of the study region.

Key words: Carbon budget, Regional climate change, MODIS, NPP, Mediterranean

INTRODUCTION

One of the key processes that drive terrestrial carbon (C) cycle at the local-to-global scales is net primary productivity (NPP). This means C gain via photosynthesis and C loss via plant respiration. Net primary productivity is a better indicator of vegetation productivity than gross primary productivity (GPP) which is impossible to directly quantify *in situ* without accounting for the simultaneous process of autotrophic respiration (Lamberty et al. 2005). Net primary productivity couples the biosphere not only to the atmosphere but also to the pedosphere, thus influencing both rate variables e.g. latent heat fluxes, litterfall, soil respiration, and nitrogen (N) mineralization and state variables e.g. soil organic and vegetation C and N pools, and atmospheric CO_2 concentration (Prentice et al. 2000; Tang et al. 2010). Significant alterations of local C cycles due to burning of fossil fuels, and land-use and land-cover changes have cumulatively enhanced the greenhouse effect, and thus, have resulted in global climate change (Potter et al. 2006). Increased air temperature, altered precipitation regime, and increased frequency of extreme climatic events have in turn triggered changes in the structure and function of terrestrial and aquatic ecosystems (IPCC 2013). The 5th Assessment Report (AR5) of the Intergovernmental Panel on Climate Change (IPCC) developed future climate change scenarios representative of possible greenhouse gas (GHG) and aerosol concentrations to reach a particular radiative forcing (W/m^2) in 2100 called "Representative Concentration Pathways (RCPs)" (IPCC 2013).

Quantification and prediction of biome NPP and its spatiotemporal responses to future regional climate

*Corresponding author E-mail: cdonmez@cu.edu.tr

change scenarios are of great importance to policy makers, institutions of natural resource management, and stakeholders to secure and enhance C sequestration potential of terrestrial and aquatic biomes (Wang et al. 2011; Evrendilek, 2014). This is in particular true for biological productivity and diversity of Mediterranean biomes whose vulnerability to climate change has been already high due to the combined effects of aridity and anthropogenic disturbances that existed historically. Direct *in situ* measurements of biome NPP are limited by cost, time, and spatiotemporal coverages, whereas NPP estimates based on remote sensing and biogeochemical models provide information in time and space series at wide ranges of spatiotemporal resolutions (Houghton 2005; Tang et al. 2010). Various biogeochemical models have been used to quantify impacts of regional climate change projections over the Mediterranean biomes on magnitude, rate, and direction of changes in NPP. However, to the authors' best knowledge; there exist no process-based modeling studies about spatiotemporal NPP dynamics over the vast areas of complex Mediterranean terrain in Turkey. The objectives of this study were to quantify NPP for the entire eastern Mediterranean biomes of Turkey using Carnegie Ames Stanford Approach (CASA) model and Moderate Resolution Imaging Spectroradiometer (MODIS) data in response to the four RCP climate change scenarios.

MATERIAL & METHODS

Study region: The eastern Mediterranean region of Turkey covers an area of ca. 76123 km^2 (38% of the entire Turkish Mediterranean region of 198165 km^2) and has the characteristic Mediterranean climate with mild, rainy winters and hot, dry summers (Fig. 1). The altitudinal range of the study region varies between 0 m and 3700 m above sea level (Fig. 1), with mean annual minimum and maximum values ranging from 375 mm to 1003 mm for rainfall and from -2 ^{o}C to 19 ^{o}C for air temperature, respectively (Fig. 2). The region has mountainous terrain with diverse micro climate and Mediterranean vegetation belts, with the neighboring Taurus Mountain range separating it from the central Anatolian steppe. Major evergreen needle leaf tree species are Pinus nigra, Pinus brutia, Cedrus libani, Abies cilicica, and Juniperus excels, while deciduous broadleaf tree species include Fagus orientalis, Quercus cerris, Fraxinus ornus, and Carpinus orientalis (Yilmaz 1998; Donmez et al. 2011). Dominant shrubland species include both maquis elements (e.g. Quercus coccifera, Arbutus unedo, Phillyrea latifolia, Pistacia lentiscus, Juniperus oxycedrus, Mrytus communis, Ceratonia siliqua, Spartium junceum, Nerium oleander, and Laurus nobilis) and garrigue elements (e.g. Cistus salvifolius, and Sarcopoterium spinosum), while dominant herbaceous species of grassland include Triticum dicoccoides, Alopecurus myosuroides, Hordeum bulbosum, Bromus intermedius, Trifolium campestre, and Acantholimon and Astragalus species (Ozturk et al. 2002).

Model description: The CASA model was used to estimate present and future spatiotemporal dynamics of annual and monthly biome NPP in the study region at a 250-m resolution as a function of absorbed photosynthetically active radiation (APAR), and mean light use efficiency (ε) as follows (Potter et al. 1993, 2003):

$$NPP = APAR \; x \; \varepsilon$$

$$NPP = f(NDVI) x \; PAR \; x \; \varepsilon \; x \; g(T) \; x \; h(W)$$

where APAR (MJ/m^2/month) is a function of normalized difference vegetation index (NDVI) (APAR/PAR H" NDVI), and down welling photosynthetically active radiation (PAR, MJ/m^2/month), while ε (in g C/MJ) is a function of the maximum achievable light utilization efficiency. Light use efficiency is adjusted by such stress-induced reduction factors as temperature [g(T)] and water [h(W)] (Potter et al., 2004). In addition, the maps of percent tree cover, land use/cover, and soil texture were used to run the model at a 250-m spatial resolution on a monthly basis. A flow chart of the methodology is shown in Fig. 2.

NPP models driven by satellite data have many advantages over models driven only by climate and/or resources both for detecting global change and for yielding temporally and spatially resolved fields of NPP. The biological basis of the links between the inputs and the outputs for a model like CASA are feasible since they use actual data set including several biophysical variables such as land cover, soils and topography (Field et al., 1995). In this regard, the CASA model was chosen in this study to estimate regional NPP dynamics in a complex Mediterranean region.

Remotely sensed imagery: Remotely sensed data used in this study were based on MODIS 16-day composite data obtained from the National Aeronautics and Space Administration (NASA) at a 250-m spatial resolution with 36 spectral bands (NASA 2013). A total of 71 MODIS images acquired between 01.04.2000 and 31.10.2014 were used for land use/cover classification. The following spectral bands are primarily used for analyses of vegetation and land surface in land use/cover classification: blue (459–479 nm), green (545–565 nm), red (620–670 nm), near infrared (841–875 nm and 1230–1250 nm), and shortwave infrared (1628–1652 nm and 2105–2155 nm) (Gobron et al. 2000, Wang et al.

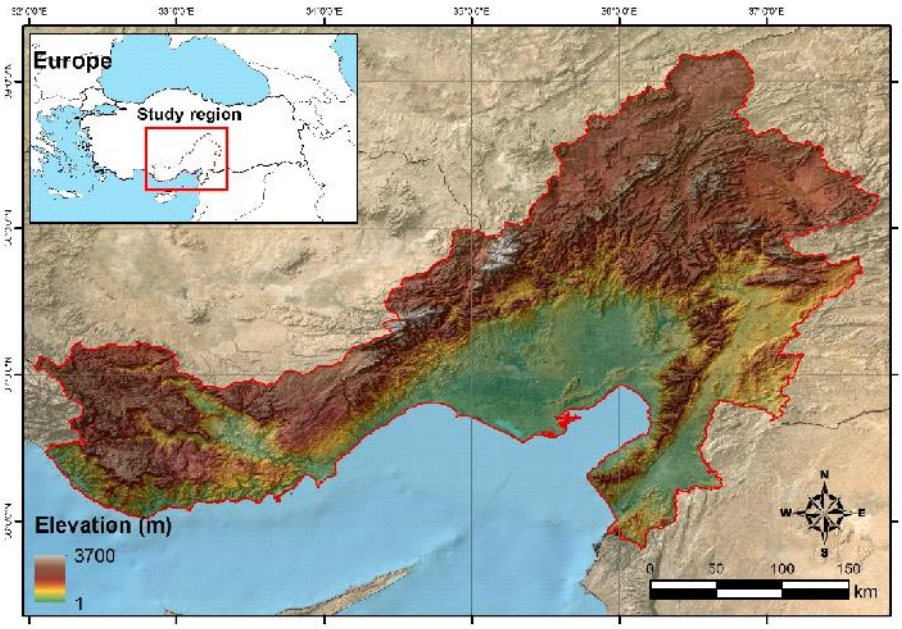

Fig. 1. Location of the eastern Mediterranean region of Turkey

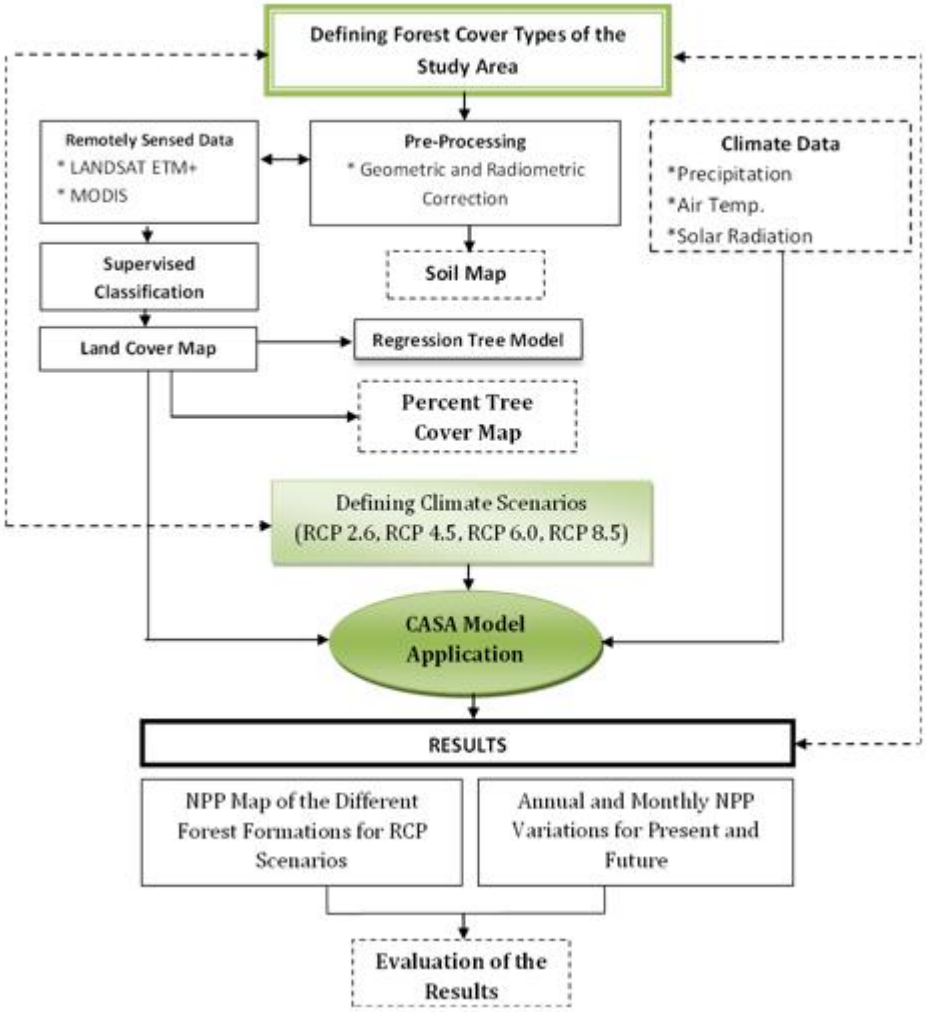

Fig. 2. Flow chart of the metholodology.

2013). These images were geometrically corrected according to WGS 84 Datum and the ED 1950 coordinate system. The MODIS/Terra NDVI images (L3 Global) at a 250-m spatial resolution were extracted and inputted to the CASA model for the study area in order to account for spatiotemporal variations in APAR and photosynthetic activity.

Present and future climate data: Daily meteorological data between 01.01.2000 and 31.12.2010 used in this study were obtained from 69 meteorological stations and included rainfall, solar radiation, and air temperature (Turkish State Meteorological Service, 2012). The daily meteorological data were aggregated on a monthly basis, co-krigged using Digital Elevation Model (DEM) and inputted into the CASA model as the main driving variables at a 250-m spatial resolution. Future climate projections for changes in temperature and rainfall by the year 2100 for the eastern Mediterranean region of Turkey were derived from the HadGEM2-ES simulations driven by the four RCPs at a 1-km spatial resolution described below. These climate change simulations were obtained from the WorldClim research group (WorldClim 2013) and were downscaled to a 250-m spatial resolution and inputted to the CASA model. The HadGEM2-ES global model is based on a fully coupled atmosphere-ocean general circulation model (HadGEM2) developed by the UK Met Office Hadley Centre, with additional dynamic representation of global-scale biogeochemical processes of terrestrial and aquatic ecosystems, at an atmospheric resolution of $1.875^{o} \times 1.25^{o}$ with 38 vertical levels, and at a temporal resolution of 30 min (Collins et al. 2011; Jones et al. 2011).

The RCP projections are the most recent climate change projections developed in the Fifth Assessment of the IPCC report as part of the Coupled Model Intercomparison Project Phase 5 (CMIP5) (Hijmans et al. 2005; WorldClim 2013). The four climate change scenarios were generated by four integrated assessment models as follows: RCP 2.6 by Integrated Model to Assess the Global Environment (IMAGE) (van Vuuren et al. 2007), RCP 4.5 by Mini-Climate Assessment Model (MiniCAM) (Clarke et al. 2007), RCP 6.0 by Asia-Pacific Integrated Model (AIM) (Hijioka et al. 2008), and RCP 8.5 by Model for Energy Supply Strategy Alternatives and their General Environmental Impact (MESSAGE) (Riahi et al. 2007). The four RCPs for the 2070-2100 period, and the baseline condition for the 2000-2010 period were presented in Figs. 3 and 4 for the study region in terms of their associated spatiotemporal variations of mean atmospheric CO_2 concentration, air temperature and rainfall.

Ancillary data: The MODIS land cover product was used to classify vegetation types and land use/cover types according to the CORINE land classification scheme at a 250-m spatial resolution. Soil texture map at a 250-m spatial resolution was based on the FAO classification system of five classes by which one of the designations "coarse", "medium", "fine", and "very fine" or their combination was assigned to the dominant soil type based on the relative fraction of clay, silt, and sand contents present in the top 30 cm of soil (Potter et al. 2003). The classes derived from the pedotransfer rules and expert opinions, and soil classification map at a scale of 25000 were also utilized for this study. Regression Tree (RT) algorithm (Breiman et al. 1984; Loh, 2002; Tottrup et al. 2007) was used to predict percent tree cover over the study region. The maps of percent tree cover, land use/cover, and soil texture were also used at a 250-m spatial resolution prior to being fed into the CASA model.

Statistical analyses: Pearson's correlation analysis was carried out to detect strength and direction of linear relationships between measured versus estimated data. Tukey's multiple comparison test following one-way analysis of variance (ANOVA) was performed to capture significant differences in mean NPP values among the RCPs and the baseline condition. One sample *t* test was used to test significant differences between mean NPP simulated for each biome under the RCPs and mean biome NPP under the baseline condition. The significance level of $p < 0.05$ was adopted for hypothesis testing. All the statistical analyses were performed using Minitab 17.0.

RESULTS & DISCUSSION

NPP simulations under baseline condition: The land use/cover map generated in this study included the following six biomes: deciduous broadleaf forest, mixed deciduous broadleaf and evergreen needle leaf forest, evergreen needle leaf forest, grassland, shrubland, and cropland (Fig. 5). Accuracy analysis was carried out comparing the land use/cover classification map and the ground truth data collected from field campaigns (Table 1). The resulting percent tree cover map derived from RT is shown in Fig. 6. Accuracy of the percent tree cover map was defined using correlation coefficient (*r*) which was 0.76 which indicated the RT model quantified the spatial distribution of forest types within a reasonable accuracy for the study region. Our simulations under the baseline (2000-2010) climate condition across the study region showed that the Mediterranean biome NPP ranged monthly from 29 gC/m^2 for shrubland in November to 325 gC/m^2 for deciduous broadleaf forest in June during the vegetation period of April to November (Fig. 7) and spatially from close to zero for fallow or uncultivated cropland to 3.2 kgC/m^2 for

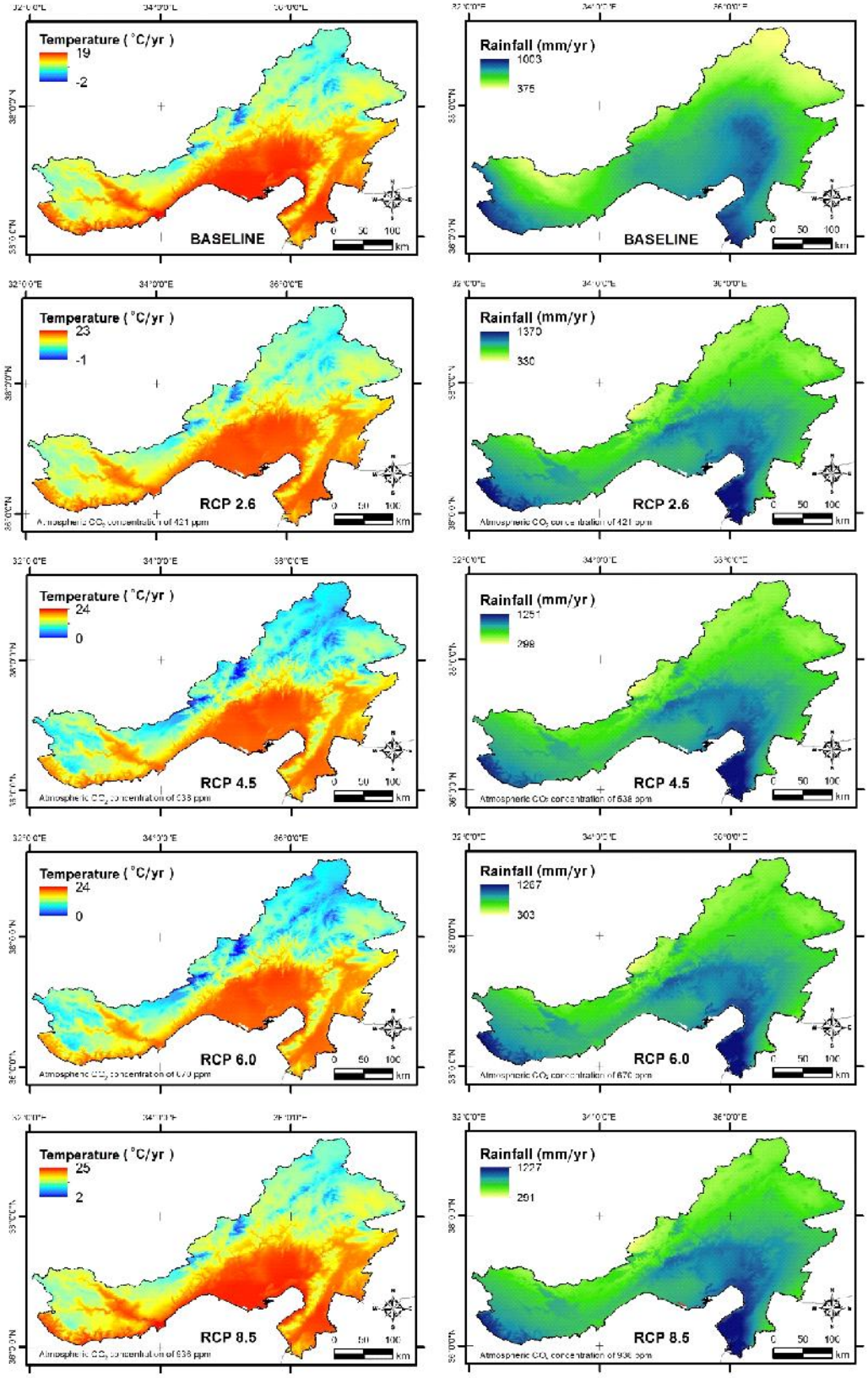

Fig. 3. A spatiotemporal comparison among the baseline (2000-2010) condition, and future (2070-2100) RCP scenarios across the eastern Mediterranean region of Turkey

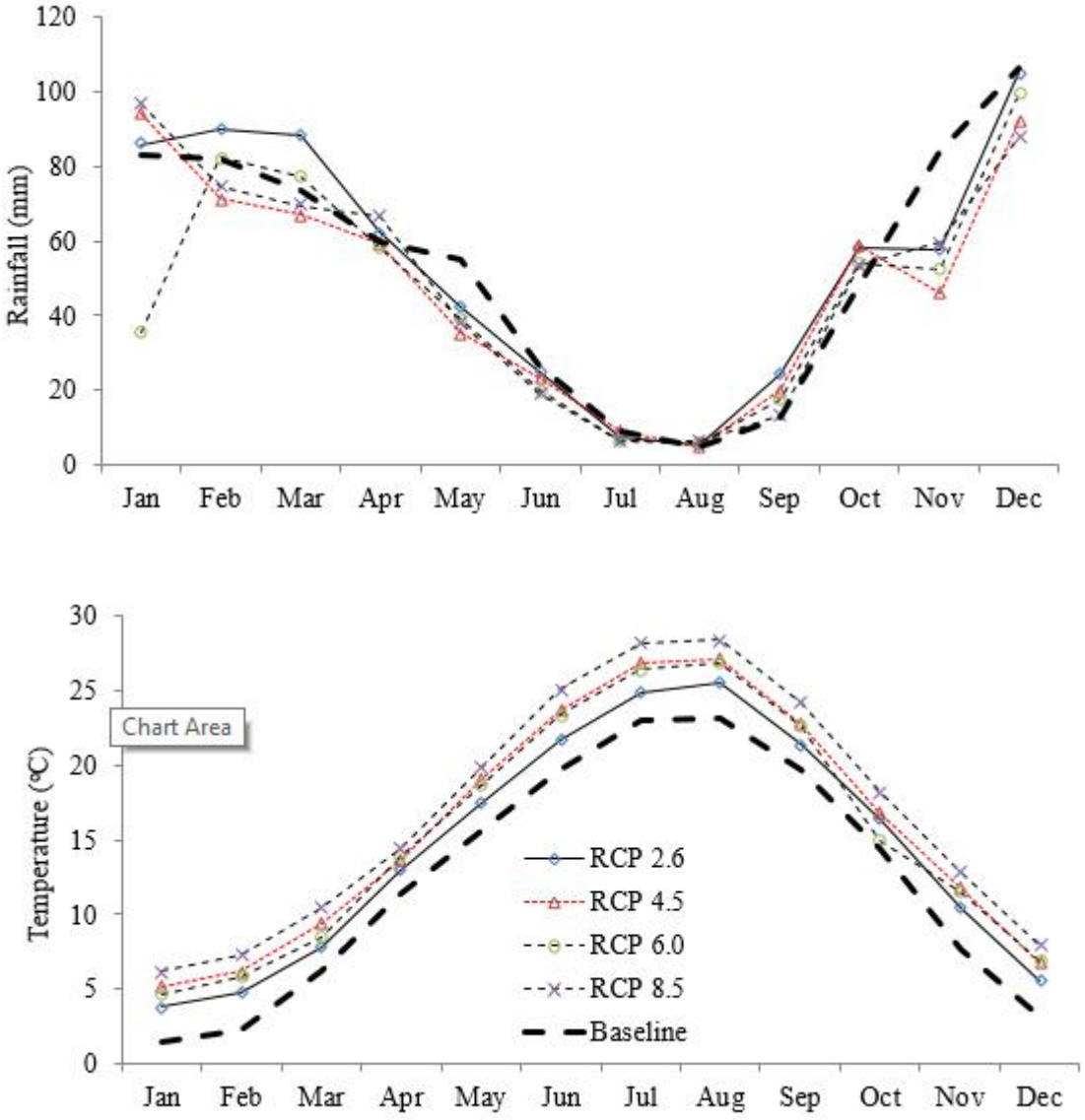

Fig. 4. Mean monthly comparisons among the baseline (2000-2010) and future (2070-2100) climate conditions in terms of air temperature and rainfall across the eastern Mediterranean region of Turkey

deciduous broadleaf forest on an annual basis (Fig. 8). Mean annual NPP under the baseline condition varied between 452 ± 244 gC/m^2 for shrubland and 1529 ± 378 gC/m^2 for deciduous broadleaf forest, with the mean terrestrial NPP of 881 ± 380 gC/m^2/yr over the different biomes (Table 2). LPJ-GUESS simulations estimated mean terrestrial biome NPP at 380 gC/m^2/yr across the EU for the 1961-1990 period (Morales et al. 2007). Cropland, shrubland, mixed forest, evergreen needle leaf forest, grassland, and deciduous broadleaf forest cover 40.0%, 23.3%, 19.5%, 7.8%, 7.6%, and 1.8% of the study region, respectively, (Table 2). The spatially varying extents of the biomes partly indicate the relative importance of their roles to the regional C cycle because their C source or sink strength depends not only on their area but also on their rate and stock limits to sequester, store and retain C in soils and vegetation over the long-term, their vulnerability to human-induced disturbances including climate change, and adoption of best management practices.

Spatiotemporal variations in climatic drivers under baseline condition and RCPs: A multiple comparison of the baseline condition (2000-2010) and the four climate change scenarios (2070-2100) is presented in Fig. 3 in terms of spatiotemporal variations in mean annual maximum and minimum air temperatures, mean annual maximum and minimum rainfall, and mean annual CO_2 concentration across the study region. Temporally, the average values of the RCPs

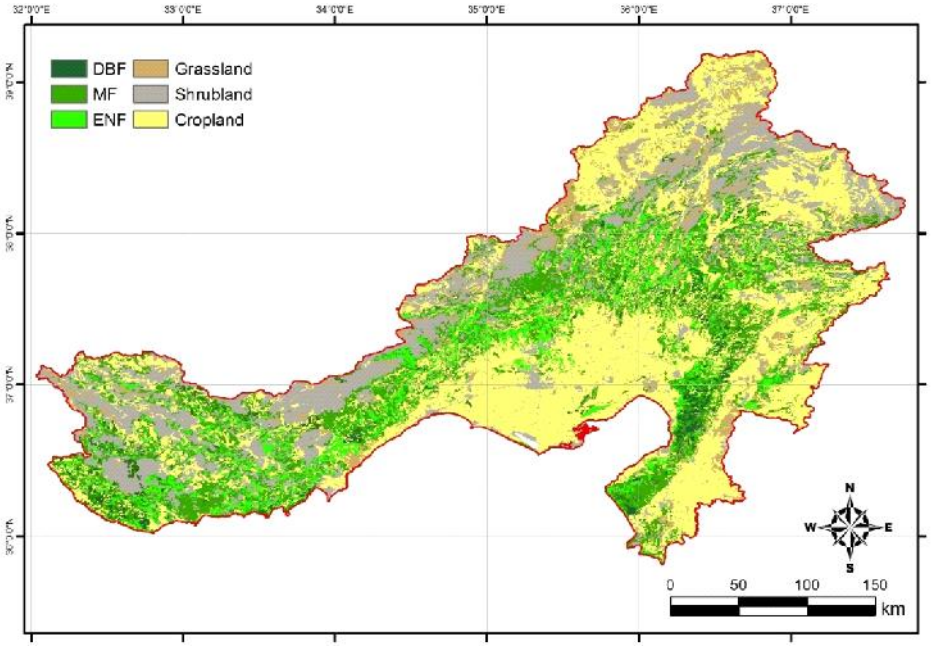

Fig. 5. Land use and land cover map of the eastern Mediterranean region of Turkey inputted into the CASA model under the baseline (2000-2010) climate conditions (DBF: Deciduous broadleaf forest, MF: Mixed deciduous broadleaf and evergreen needle leaf forest, and ENF: Evergreen needle leaf forest)

Table 1. Accuracy assessment matrix of land use/cover classification for the study region

Land cover/use	Producer's accuracy(%)	User's accuracy(%)	Kappa(%)
DBF	85	87	87
MF	78	79	81
ENF	81	79	80
Grassland	79	81	83
Shrubland	81	83	84
Cropland	86	88	89
Overall Accuracy	82		84

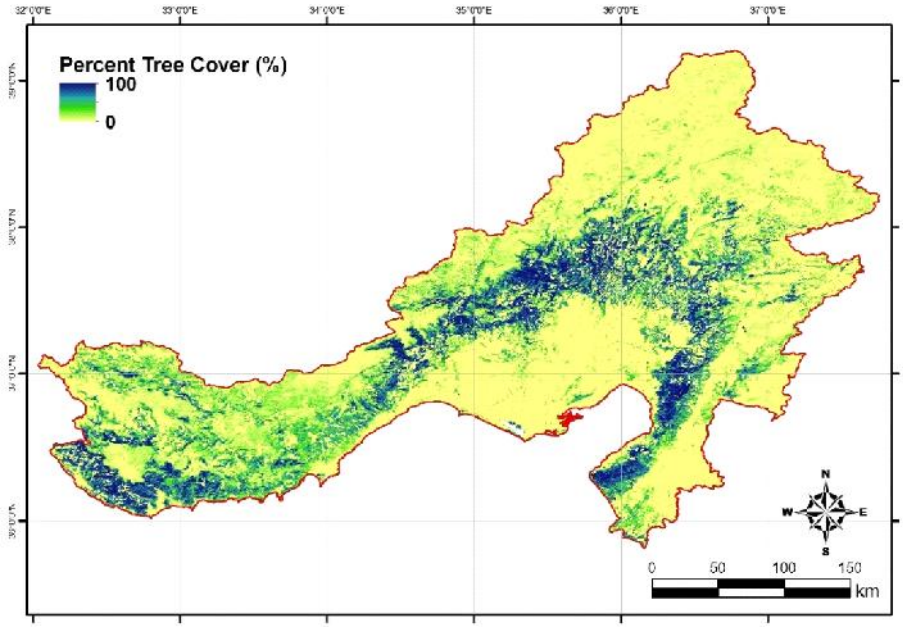

Fig. 6. Percent tree cover map of the eastern Mediterranean region of Turkey inputted into the CASA model under the baseline (2000-2010) climate conditions

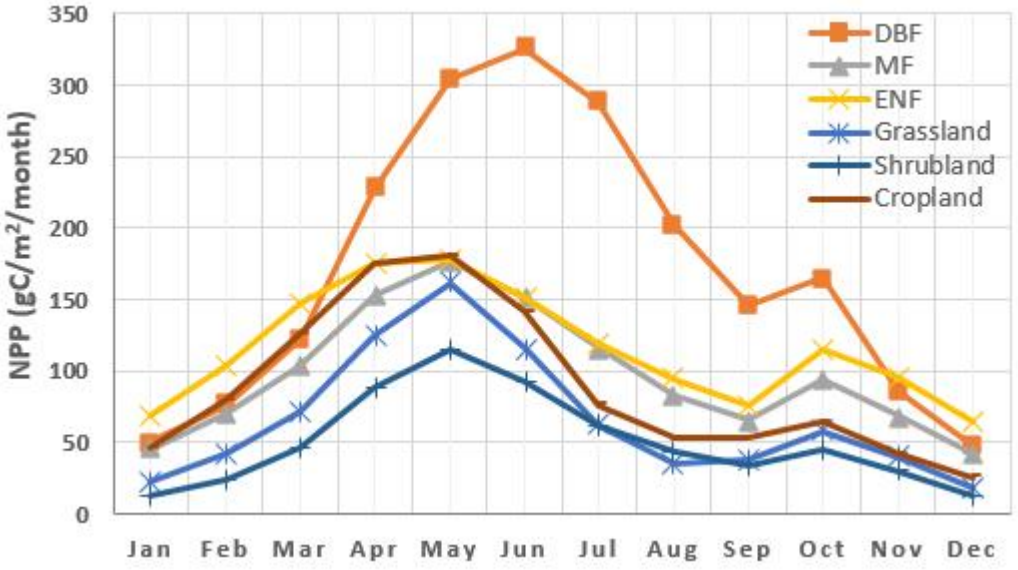

Fig. 7. Temporal dynamics of mean monthly net primary productivity (NPP) of the eastern Mediterranean biomes of Turkey simulated by the CASA model under the baseline (2000-2010) climate conditions

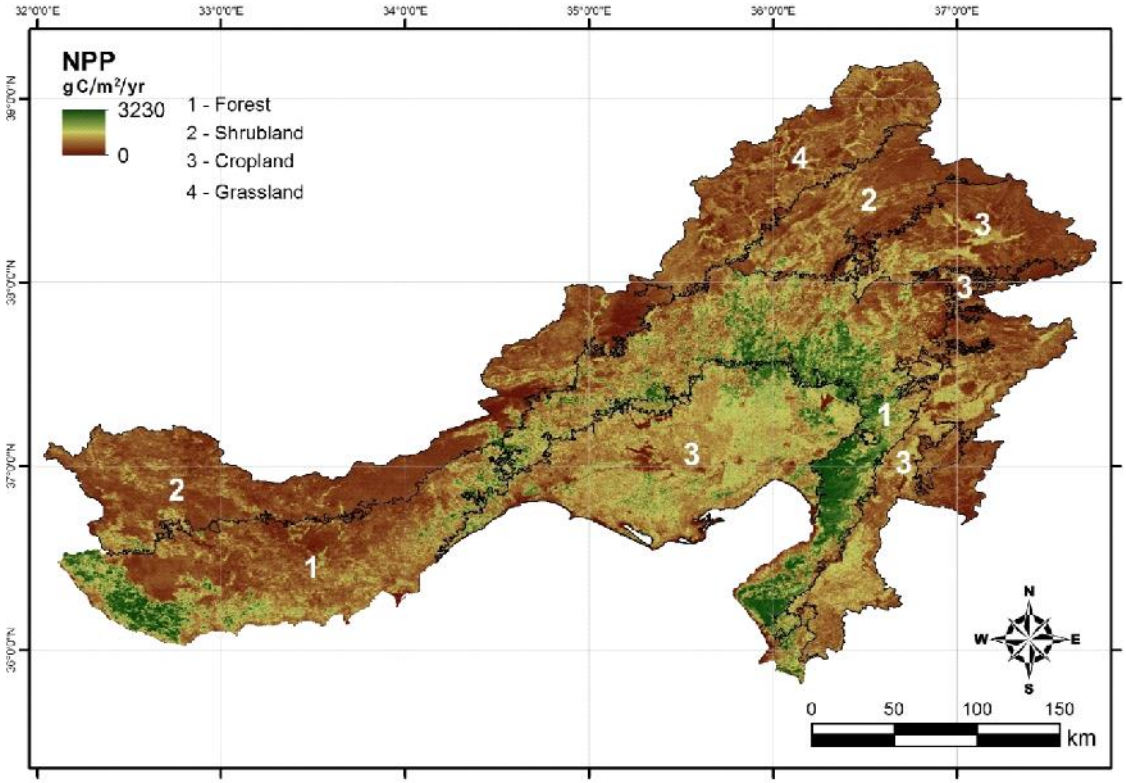

Fig. 8. Spatial dynamics of mean annual net primary productivity (NPP) of the eastern Mediterranean biomes of Turkey simulated by the CASA model for the baseline period (2000-2010)

indicated increases by 26% (5°C) and 113% (2°C) in mean annual maximum and minimum air temperatures, respectively, by 27% (276 mm) in mean annual maximum rainfall and a decrease by 18% (69 mm) in mean annual minimum rainfall. The monthly changes in mean rainfall were such that rainfall decreased during both the early-to-middle growing season from May to July and the late growing season from October to November but increased during the period of August to October (Fig. 4). Spatially, the distinct difference in rainfall

distribution between the baseline condition and the RCPs was that the spatial extent of the mean annual minimum rainfall localized along the northern edges of the study region under the baseline condition decreased significantly over the same area under the RCPs (Fig. 2). Similarly, the spatial extent of mean annual minimum temperature in the northern sections under the baseline condition increased noticeably, thus creating localized climate cooling over the same area under the RCPs 4.5 and 6.0 (Fig. 3). On a monthly scale, mean annual air temperature relative to the baseline condition was higher in increasing order in response to the RCPs 2.6, 6.0, 4.5 and 8.5, respectively. The RCP 2.6 as the lowest emission and radiative forcing scenario representative of the most severe mitigation measures limited mean minimum and maximum temperature increases to 1°C (50%) and 4°C (21%), respectively, mean minimum rainfall decrease to 45 mm (12%), and mean maximum rainfall increase to 267 mm (37%) by the 2070-2100 period. The RCP 8.5 mean minimum and maximum temperatures are projected to increase by 4°C (200%) and 6°C (32%), while the RCP 8.5 mean minimum and maximum rainfall is projected to decrease by 84 mm (22%) and to increase by 224 mm (22%), respectively, for the same time period. Mean minimum and maximum temperatures are expected to increase at the same rate by 2°C (100%) and 5°C (26%), respectively, under the intermediate climate change scenarios represented by RCP 4.5 and RCP 6.0. However, the RCP 4.5 scenario projects 16 mm less increase in mean maximum rainfall and 4 mm more decrease in mean minimum rainfall than the RCP 6.0 scenario.

NPP simulations under baseline condition versus RCPs: There was no significant difference between the baseline condition and the RCPs in terms of mean annual biome NPP ($p > 0.05$). The mean terrestrial biome NPP of the study region varied between 877 $\pm$ 360 gC/m^2/yr under RCP 2.6 and 894 $\pm$ 363 gC/m^2/yr under RCP 8.5, with the grand mean of 885 $\pm$ 7 gC/m^2/yr . The mean annual biome NPP under the baseline condition decreased by 0.5% under RCP 2.6 and increased by 0.7%, 0.1%, and 1.4% under the RCPs 4.5, 6.0 and 8.5, respectively. Bonan (2008) reported that NPP of global terrestrial biomes decreased by up to 6% $°C^{-1}$ in seven process-based models and increased by 1 to 2% $°C^{-1}$ in four process-based models. The overall slight increase in the mean present annual NPP over the study region in response to the RCPs suggests that the enhanced NPP (negative feedback) of grassland, evergreen needle leaf forest, cropland, mixed forest, and shrub land on average slightly more than offset the decreased NPP (positive feedback) of deciduous broadleaf forest. The higher mean annual NPP of all the terrestrial biomes by 0.4% under the RCPs than under the baseline condition may be attributed primarily to interaction impacts of the increases in mean annual air temperature and rainfall projected by the RCPs on NPP (Fig. 4).

When the mean annual NPP values were compared between the baseline condition and the average value of the RCPs, there was a decrease by 3.2% for deciduous broadleaf forest ($p < 0.001$), whereas increases ranging from 0.7% for shrub land ($p = 0.02$) to 2.8% for grassland ($p = 0.01$) occurred for the remaining biomes (Table 2). However, the mean annual NPP values of mixed and evergreen needle leaf forests increased by 0.9% and 2.4%, respectively, under the RCPs but did not differ significantly when compared to the baseline condition ($p > 0.05$). Morales et al. (2007) used the LPJ-GUESS process-based ecosystem model driven by 10 regional climate model-generated climate scenarios over the European Union (EU) for the 2071–2100 period. Morales et al. (2007) found that mean annual NPP increased by 14.9 $\pm$ 4.8% for the southeast Mediterranean region of the EU (35–45°N latitudes, 18–35°E longitudes) including the western Mediterranean biomes of Turkey, by 75% for evergreen needle leaf forest, and by 5% for grassland over the southwest and southeast Mediterranean EU in response to mean temperature increase by 4.8°C and mean rainfall decrease by 16.4%. A mechanistic model used by Osborne et al. (2000) simulated that evergreen sclerophyllous shrub (locally known as maquis) NPP, on average, rose by 25% in Portugal, Spain, and France during the past century owing to CO_2 fertilization and increased water use efficiency. The process-based model (GOTILWA+) simulations by Keenan et al. (2011) showed CO_2 fertilization to increase forest NPP despite increased drought stress by up to three times that of the non-CO_2 fertilization scenario by the 2050-2080 period and emphasized limits that soil organic C and nitrogen interactions pose to Mediterranean biome NPP stimulated by CO_2 fertilization. Such crop models as Daisy, CERES, and CropSyst applied to Spain by Olesen et al. (2007) so as to reflect southern European crop conditions under regional climate scenarios for 2071-2100 indicated a mean yield increase of 90% for spring wheat, but a yield decrease of 21% for both winter wheat and irrigated grain maize.

Regardless of the RCPs used, the monthly CASA model simulations indicated an increase of different magnitudes during the winter and spring (January-May) and a decrease of different magnitudes during the summer (June-September) in the NPP trajectories of all the biomes relative to the baseline condition (Figs. 89to 14). The simulated increases in mean annual NPP ranged from 0.4% with shrubland under the RCPs 2.6

and 6.0 to 4.4% with evergreen needle leaf forest under RCP 8.5. The simulated decrease in mean annual NPP varied between 0.2% with mixed forest under RCP 2.6 and 3.5% with deciduous broadleaf forest under RCP 2.6 (Table 2). This pattern suggests that deciduous broadleaf forest NPP is more vulnerable than the other biomes to the decreased rainfall and the increased air temperature of the water-limited growing season projected by the RCPs. In other words, the onset date of green-up, and thus, spring vegetation growth for deciduous broadleaf forest biomes in the study region may not be significantly coupled with the mean air temperature increase and the rainfall increase or decrease of the pre-growing season before April. However, the rising winter and spring temperatures but the change in non-growing season rainfall appeared to benefit the earlier spring green-up, and thus, spring growth of grasses, evergreen needle leaf trees, crops, and shrubs in decreasing order of magnitude. Greater vulnerability of deciduous broadleaf forest than mixed and conifer forests to the decreased growing-season rainfall between both April and August and October and November may stem from the fact that growing-season evaporative fraction defined as the ratio of evapotranspiration (latent heat flux) to available energy as an indicator of physiological stress is generally greater over deciduous broadleaf forest than over conifer forest (Piao et al. 2006; Bonan 2008). Sabate et al. (2002) reported that simulation results of a process-based forest growth model (GOTILWA+) for the Mediterranean forests of *Pinus halepensis*, *P. pinaster*, *P. sylvestris*, and *Fagus sylvatica* in Italy and Spain, on average, showed 148% and 55% higher NPP values for evergreen needle leaf and deciduous broadleaf forests, respectively, in response to the mean increases in atmospheric CO_2 concentration (CO_2 fertilization) by 90%, air temperature by 40% and rainfall by 40% projected for the 2090-2100 period which were linked primarily to effects of CO_2 fertilization, and extended growing season. As a consequence of this future NPP response of deciduous broadleaf forest, a shift from deciduous broadleaf forest toward conifer forest may become more widespread, in particular, in the southern, low-altitude areas of the study region.

NPP simulations under RCPs: There was no significant difference among the RCPs in terms of mean annual biome NPP ($p > 0.05$). The two extreme projections of RCP 8.5 (the business-as-usual GHG emissions scenario) and RCP 2.6 (the most severe mitigation measures) climate change scenarios exerted the most and least prominent influences on annual and monthly NPP values of all the biomes relative to the baseline condition, respectively (Figs. 8 to 13) (Table 2). Out of all the RCPs, the RCP 8.5-driven CASA simulations of mean annual NPP led to the most

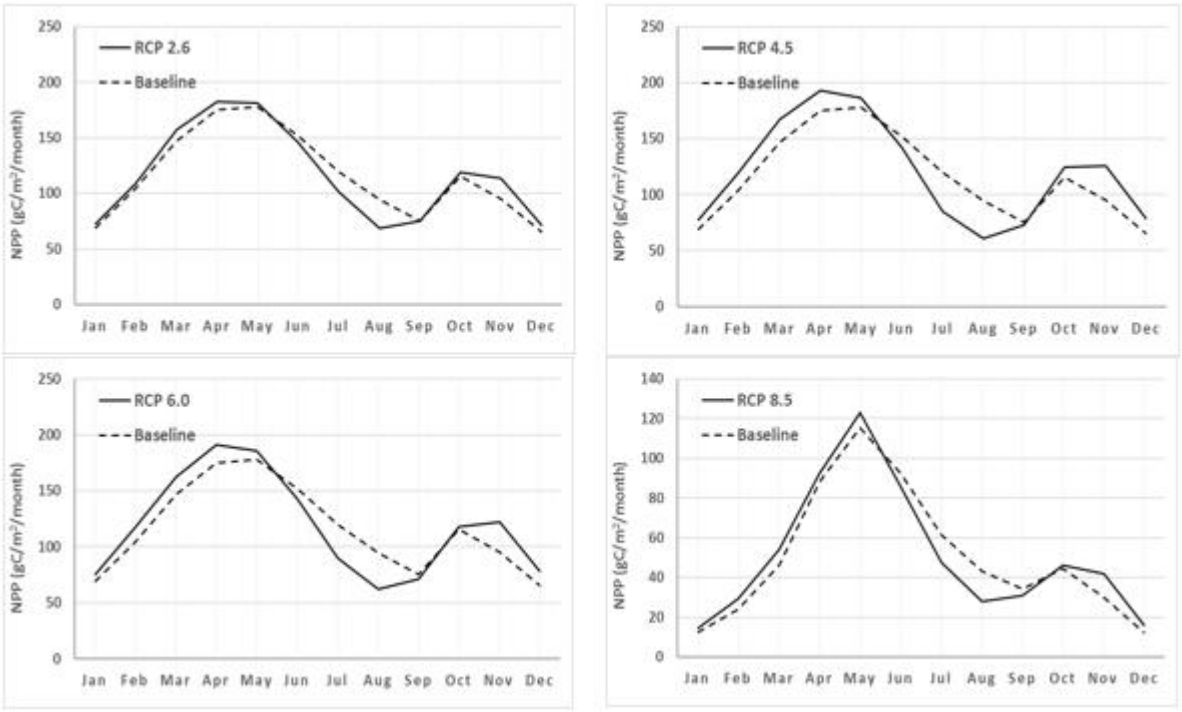

Fig. 9. Temporal net primary productivity (NPP) dynamics of evergreen needle leaf forest under the baseline climate condition and the four RCP scenarios

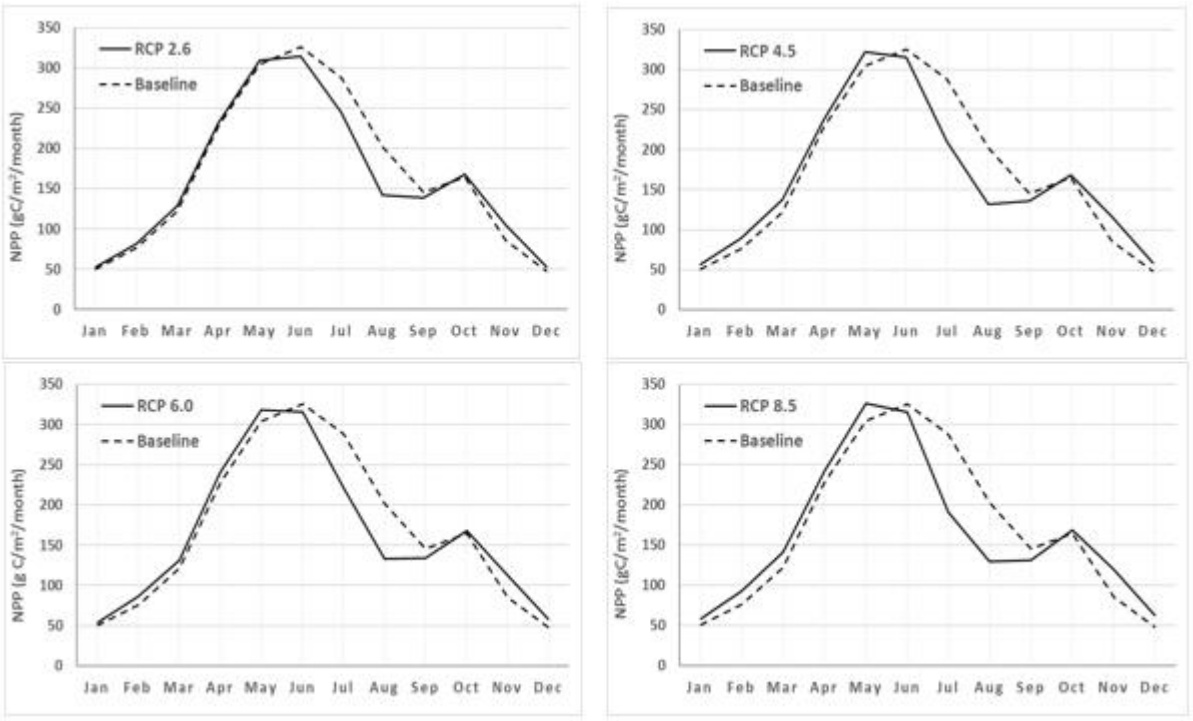

Fig. 10. Temporal net primary productivity (NPP) dynamics of deciduous broadleaf forest under the baseline climate condition and the four RCP scenarios

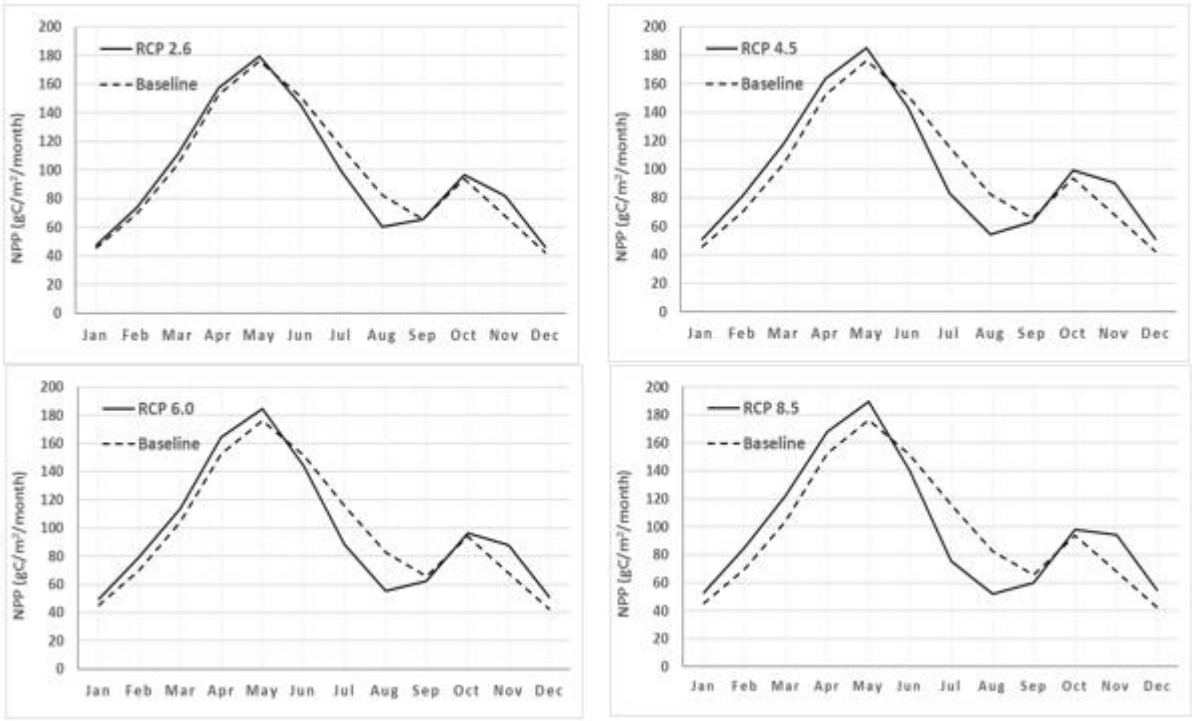

Fig. 11. Temporal net primary productivity (NPP) dynamics of mixed deciduous broadleaf and evergreen needle leaf forest under the baseline climate condition and the four RCP scenarios

increases by 4.4% with evergreen needle leaf forest, by 3.9% with grassland, by 3.4% with cropland, by 2.2% with mixed forest, and by 1.1% with shrubland and to the least decrease by 3% with deciduous broadleaf forest. On the contrary, the mean annual NPP simulations under the RCP 2.6 projection resulted in the least increases by 1.7% with grassland, by 1.1% with cropland, by 0.6% with evergreen needle leaf forest,

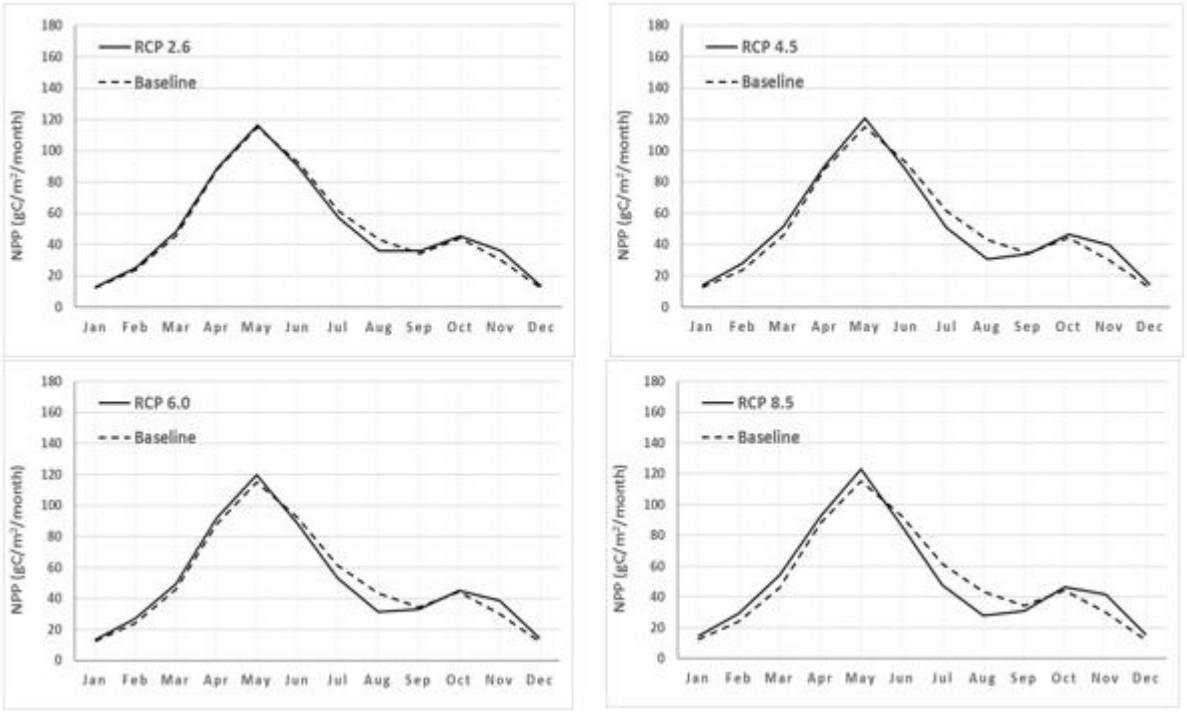

Fig. 12. Temporal net primary productivity (NPP) dynamics of grassland under the baseline climate condition and the four RCP scenarios

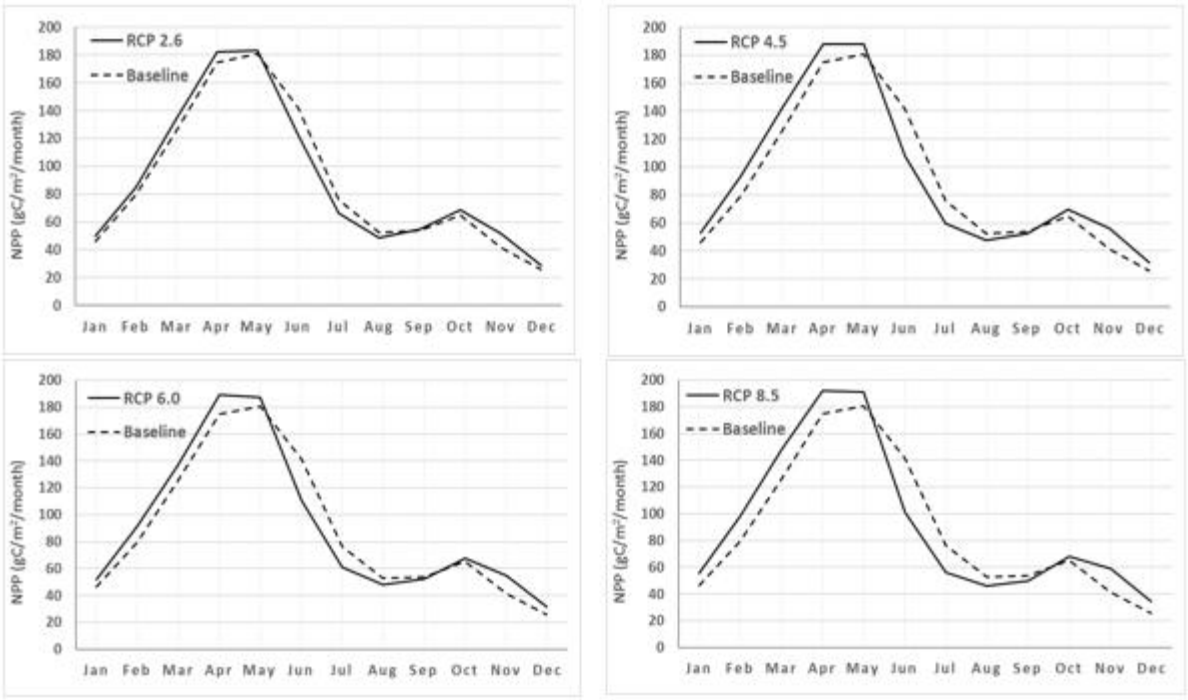

Fig. 13. Temporal net primary productivity (NPP) dynamics of cropland under the baseline climate condition and the four RCP scenarios

and by 0.4% with shrubland and in the most decreases by 3.5% with deciduous broadleaf forest, and by 0.2% with mixed forest.

Given the similar spatiotemporal distribution of temperature and rainfall under the RCPs 2.6 and 8.5 (Figs. 2 and 3), the higher mean annual biome NPP values under RCP 8.5 than RCP 2.6 can be attributed mainly to the higher magnitudes of the mean minimum and maximum temperature increases, and the resulting narrower temperature range (minimum minus maximum)

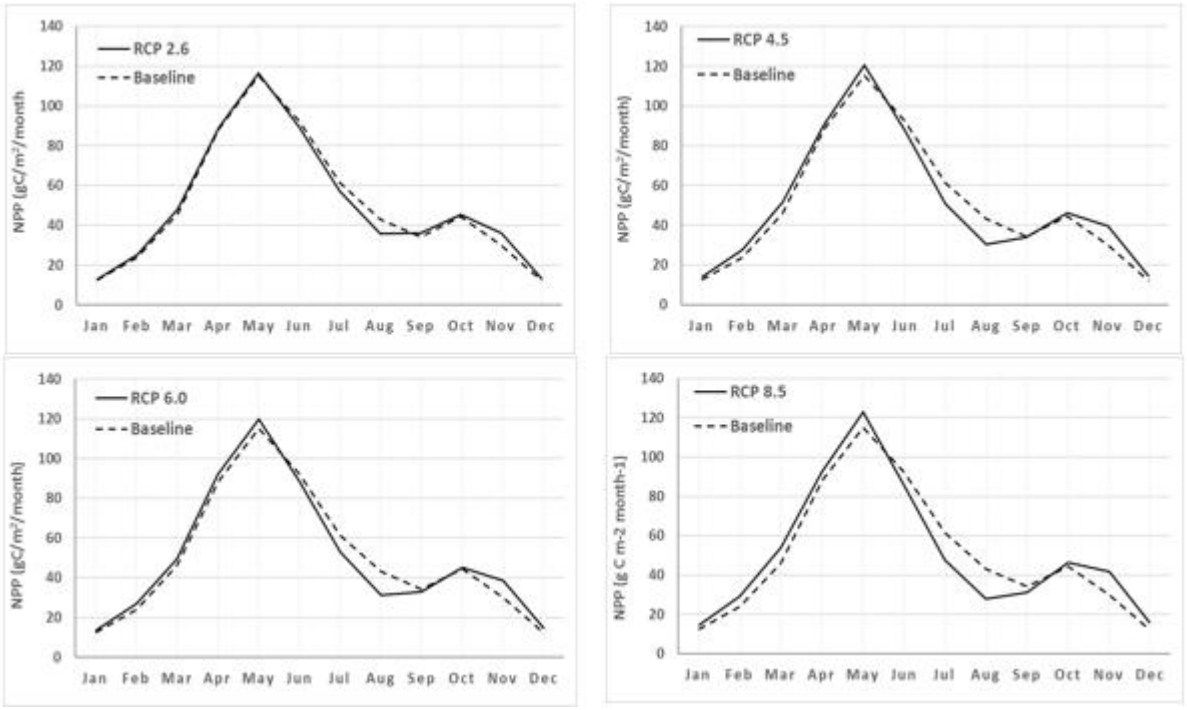

Fig. 14. Temporal net primary productivity (NPP) dynamics of shrubland under the baseline climate condition and the four RCP scenarios

Table 2. Mean annual net primary productivity (NPP, gC/m²/yr) of the eastern Mediterranean biomes under the baseline and RCP climate scenarios

Land use/cover		Mean NPP (gC/m²/yr) in 2000-2010	Mean NPP (gC/m²/yr) in 2070-2100				Grand mean change (%)
	Area (km²)	Baseline	RCP 2.6	RCP 4.5	RCP 6.0	RCP 8.5	
DBF	1402	1529 ± 378	1476 ± 360	1482 ± 362	1480 ± 362	1483 ± 363	-3.2
MF	14873	876 ± 233	874 ± 233	887 ± 241	881 ± 237	895 ± 246	0.9
ENF	5911	1042 ± 257	1048 ± 258	1073 ± 267	1061 ± 263	1088 ± 273	2.4
Grassland	5754	591 ± 174	601 ± 177	610 ± 181	605 ± 180	614 ± 184	2.8
Shrubland	17699	452 ± 244	454 ± 249	456 ± 255	454 ± 253	457 ± 260	0.7
Cropland	30484	797 ± 80	806 ± 70	817 ± 75	812 ± 60	824 ± 69	2.2
Grand total/mean	76123	881 ± 380	877 ± 360	888 ± 362	882 ± 362	894 ± 363	0.4

under RCP 8.5 (23°C/yr) than RCP 2.6 (24°C/yr). Annually, 3°C higher mean minimum temperature and 2°C higher maximum temperature (the narrower temperature range) under RCP 8.5 than RCP 2.6 are most likely to have extended the length of the growing season, thus, increased all the biome NPP values by 1.9% more under RCP 8.5 than RCP 2.6. For example, Chmielewski and Rotzer (2001) found that an early winter or spring (February to April) warming of 1 °C advanced the beginning of growing season by 7 days. There was a smaller difference in mean annual biome NPP values between the RCPs 4.5 and 6.0 than between the RCPs 2.6 and 8.5. The slightly (0.6%) higher mean annual NPP value over the biomes under RCP 4.5 with lower mean annual minimum and maximum rainfall than under RCP 6.0 is most likely to result from the slightly higher mean monthly temperature under RCP 4.5 than under RCP 6.0, given the similar spatiotemporal distribution of temperature and rainfall. The spatial extent of NPP differences between the baseline condition and each of the RCPs according to the aggregated biome classification shows the maximum

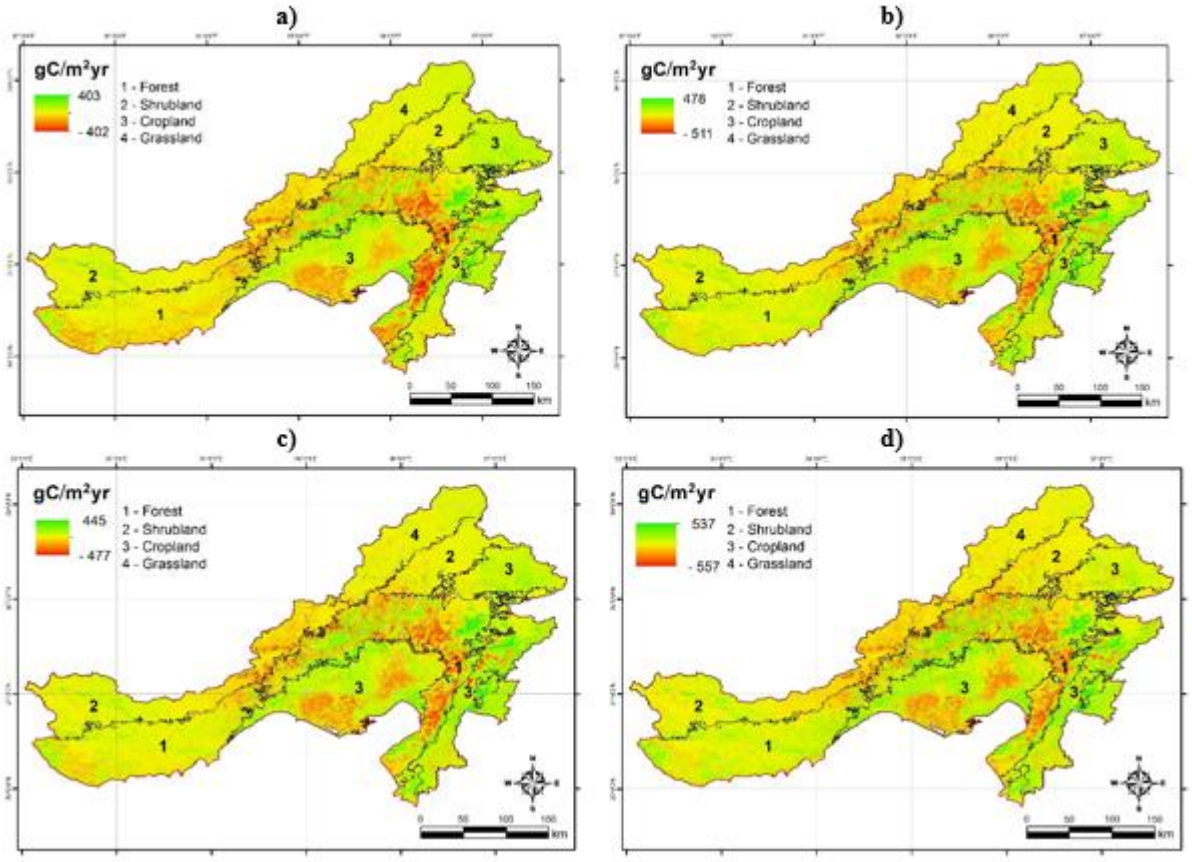

Fig. 15. Spatiotemporal difference in mean annual biome NPP between the baseline (2000-2010) and future (2070-2100) climate conditions according to (a) RCP 2.6, (b) RCP 4.5, (c) RCP 6.0, and (d) RCP 8.5

NPP decrease concentrated in the Middle Eastern parts where forests mostly exist and the maximum NPP increase in the eastern parts where forests and cropland mostly exist (Fig. 15).

CONCLUSIONS

The combined use of the CASA model, the MODIS data, and the interpolations of the baseline conditions and the regional climate change scenarios (RCP 2.6, RCP 4.5, RCP 6.0, RCP 8.5) yielded regional-scale insight into spatiotemporal NPP responses of the eastern Mediterranean biomes of Turkey between 2000-2010 and 2070-2100. The present study revealed that mean annual NPP increased for all the biomes except for deciduous broadleaf forest though not significant relative to the baseline condition. Our results showed a clear discrepancy of trajectory between deciduous broadleaf forest and the other biomes in terms of their NPP response to the RCPs. The present study did not take into account changes in biome redistribution, CO_2 fertilization effect, soil nutrients and water, land use/cover, and management practices. In the future studies, interaction effects of the driving variables (e.g. CO_2 fertilization, changes in minimum and maximum daytime versus nighttime temperatures, and management practices) should be quantified not only on all the ecosystem compartments (e.g. soil organic C pools, and soil water content) but also on both ecosystem structure (e.g. biodiversity, and herbivory) and function (e.g. nutrient and water cycles).

Under the RCP 2.6 scenario, annual NPP decreases from -53 gC/m^2/yr for DBF formations whereas under the RCP 4.5 scenario, annual NPP is up to -47 gC/m^2/yr. The results under both scenarios show that the larger decreases in NPP mainly occur in DBF formation, NPP of Grasslands is expected to increase approx. +2.8 % in total. Moreover, NPP of the land cover types of the study are will show a slight increase under RCP scenarios in future. Our study also indicated a strong correlation between and climate variables and regional NPP. Temperature is a key factor which significantly effects forest growth in the south part of the area. Both temperature and rainfall might be key factors on NPP. Temperature has the greater impact on NPP in karst areas particularly in Mediterranean regions. These analysis of the interactions among NPP and climate

variables has contributed to our understanding of vegetation productivity, especially in a complex Mediterranean watershed.

ACKNOWLEDGEMENTS

This study was financially supported by the Scientific and Technological Research Council of Turkey (TUBITAK) (Grant No. CAYDAG-110Y338, TOVAG-JPN-04-103O011 and CAYDAG-114Y273) and by the Scientific Research Project Administration Units of Cukurova University (Grant No. ZF2010D8).

REFERENCES

Bonan, G.B. (2008). Forests and climate change: forcings, feedbacks, and the climate benefits of forests. Science, **320,** 1444–1449.

Breiman, L., Friedman, J., Olshen, R.C. and Stone, C. (1984). Classification and Regression Trees. Chapman and Hall, New York.

Chmielewski, F.M. and Rotzer, T. (2001). Response of tree phenology to climate change across Europe. Agr. Forest Meteorol., **108,** 101–112.

Clarke, L., Edmonds, J., Jacoby, H., Pitcher, H., Reilly, J. and Richels, R. (2007). Scenarios of Greenhouse Gas Emissions and Atmospheric Concentrations. U.S. Climate Change Science Program and the Subcommittee on Global Change Research Synthesis and Assessment Product 2.1.

Collins, W.J., Bellouin, N., Doutriaux-Boucher, M., Gedney, N., Halloran, P., Hinton, T., Hughes, J., Jones, C.D., Joshi, M., Liddicoat, S., Martin, G., O'Connor, F., Rae, J., Senior, C., Sitch, S., Totterdell, I., Wiltshire, A. and Woodward, S. (2011). Development and evaluation of an Earth-System model–HadGEM2. Geosci. Model Dev., **4,** 1051–1075.

Donmez, C., Berberoglu, S. and Curran, P.J. (2011). Modelling the current and future spatial distribution of net primary production in a Mediterranean watershed. Int. J. Appl. Earth Obs. Geoinf. **6,** 336–345.

Evrendilek, F. (2014). Modeling net ecosystem CO_2 exchange using temporal neural networks after wavelet denoising. Geogr. Anal **46,** 37–52.

Field, C.B., Randerson, J.T. and Malmstrom, C.M., (1995). Global Net Primary Production: Combining Ecology and Remote Sensing, Remote Sensing Environment, 51:74-88.

Gobron, N., Pinty, B., Verstraete, M.M. and Widlowski, J. L. (2000). Advanced spectral algorithm and new vegetation indices optimized for upcoming sensors: development, accuracy and applications. IEEE Trans. Geosci. Remote Sens., **38,** 2489–2505.

Hijioka, Y., Matsuoka, Y., Nishimoto, H., Masui, M. and Kainuma, M. (2008). Global GHG emissions scenarios under GHG concentration stabilization targets. J. Global Environ. Eng. **13,** 97–108.

Hijmans, R.J., Cameron, S.E., Parra, J.L., Jones, P.G. and Jarvis, A. (2005). Very high resolution interpolated climate surfaces for global land areas. Int. J. Climatol., **25,** 1965–1978.

Houghton, R.A. (2005). Aboveground forest biomass and the global carbon balance. Global Change Biol. **11,** 945–958.

IPCC. (2013). Summary for Policymakers. In: Climate Change. The Physical Science Basis. Contribution of Working Group I to the Fifth Assessment Report of the Intergovernmental Panel on Climate Change, edited by: Stocker, T.F., Qin, D., Plattner, G.-K., Tignor, M., Allen, S.K., Boschung, J., Nauels, A., Xia, Y., Bex, V., and Midgley, P.M., Cambridge University Press, Cambridge.

Jones, C.D., Hughes, J.K., Bellouin, N., Hardiman, S.C., Jones, G.S., Knight, J., Liddicoat, S., O'Connor, F.M., Andres, R.J., Bell, C., Boo, K.O., Bozzo, A., Butchart, N., Cadule, P., Corbin, K.D., Doutriaux-Boucher, M., Friedlingstein, P., Gornall, J., Gray, L., Halloran, P.R., Hurtt, G., Ingram, W., Lamarque, J.F., Law, R.M., Meinshausen, M., Osprey, S., Palin, E.J., Parsons Chini, L., Raddatz, T., Sanderson, M., Sellar, A.A., Schurer, A., Valdes, P., Wood, N., Woodward, S., Yoshioka, M., Zerroukat, M. (2011). The HadGEM2-ES implementation of CMIP5 centennial simulations. Geosci. Model Dev., **4,** 543–570.

Keenan, T., Maria Serra, J., Lloret, F., Ninyerola, M. and Sabate, S. (2011). Predicting the future of forests in the Mediterranean under climate change, with niche- and process-based models: CO_2 matters!. Global Change Biol. **17,** 565–579.

Lambertyü B., Stith T., Gower, S., Douglas, E. and Thornton, P. (2005). Reimplementation of the Biome-BGC model to simulate successional change. Tree Physiol., 25, 413–424.

Loh, W.Y. (2002). Regression trees with unbiased variable selection and interaction detection. Stat. Sinica, **12,** 361–386.

Morales, P., Hickler, T., Rowell, D.P., Smith, B. and Sykes, M.T. (2007). Changes in European ecosystem productivity and carbon balance driven by regional climate model output. Global Change Biol., **13,** 108–122.

NASA, (2013). Land Processes Distributed Archive Center Web Site, https://lpdaac.usgs.gov. Accessed 12 October 2014.

Olesen, J.E., Carter, T.R., Diaz-Ambrona, C.H., Fronzek, S., Heidmann, T., Hickler, T., Thomas, L.U., Holt, T., Minguez, M.I., Morales, P., Palutikov, J., Quemada, M., Ruiz-Ramos, M., Rubæk, G.H., Sau, F., Smith, B. and Sykes, M.T. (2007). Uncertainties in projected impacts of climate change on European agriculture and terrestrial ecosystems based on scenarios from regional climate models. Climatic Change, 81: 123-143.

Osborne, C.P., Mitchell, P.L., Sheehy, J.E. and Woodward, F.I. (2000). Modelling the recent historical impacts of atmospheric CO_2 and climate change on Mediterranean vegetation. Global Change Biol., 6, 445–458.

Ozturk, M., Celik, A., Yarci, C., Aksoy, A. and Feoli, E. (2002). An overview of plant diversity, land use and degradation in the Mediterranean region of Turkey. Environ. Manage. Health, **13,** 442–449.

Piao, S., Fang, J., Zhou, L., Ciais, P. and Zhu, B. (2006). Variations in satellite-derived phenology in China's temperate vegetation. Global Change Biol., **12,** 672–685.

Potter, C.S., Randerson, J.T., Field, C.B., Matson, P.A., Vitousek, P.M., Mooney, H.A. and Klooster, S.A. (1993). Terrestrial ecosystem production: A process model based on global satellite and surface data. Global Biogeochem. Cy. **7,** 811–841.

Potter, C., Klooster, S., Steinbach, M., Tan, P., Kumar, V., Shekhar, S., Nemani, R. and Myneni, R. (2003). Global teleconnections of climate to terrestrial carbon flux. J. Geophys. Res., **108,** 4556.

Potter, C.S., Klooster, S., Steinbach, M., Tan, P., Sheikarand, S. and Carvalho, C. (2004). Understanding global teleconnections of climate to regional model 13 estimates of Amazon ecosystem carbon fluxes. Global Change Biol., **10,** 693–703.

Potter, C., Klooster, S., Nemani, R, Genovese, V., Hiatt, S., Fladeland, M., Gross, P. (2006). Estimating carbon budgets for U.S. ecosystems. EOS **87,** 85–96.

Prentice, I.C., Heimann, M. and Sitch, S. (2000). The carbon balance of the terrestrial biosphere: Ecosystem models and atmospheric observations. Ecol. Appl., **10,** 1553–1573.

Riahi, K., Gruebler, A. and Nakicenovic, N. (2007). Scenarios of long term socio-economic and environmental development under climate stabilization. Technol. Forecast. Soc., **74,** 887–935.

Sabate, S., Gracia, C.A. and Sanchez, A. (2002). Likely effects of climate change on growth of Quercus ilex, Pinus halepensis, Pinus pinaster, Pinus sylvestris and Fagus sylvatica forests in the Mediterranean region. Forest Ecol. Manag., **162,** 23–37.

Tang, G., Beckage, B., Smith, B. and Miller, P.A. (2010). Estimating potential forest NPP, biomass and their climatic sensitivity in New England using a dynamic ecosystem model. Ecosphere, **1,** 1–20.

Tottrup, C., Rasmussen, M.S., Eklundh, L. and Jönsson, P. (2007). Mapping fractional forest cover across the highlands of mainland Southeast Asia using MODIS data and regression tree modelling. Int. J. Remote Sens., **28,** 23–46.

Turkish State Meteorological Service (2012). Turkish Meteorological Data Archive and Management System (**TUMAS**). Available at http://tumas.mgm.gov.tr/wps/portal/ Accessed 12 October 2014.

van Vuuren, D., den Elzen, M., Lucas, P., Eickhout, B., Strengers, B., van Ruijven, B., Wonink, S. and van Houdt, R. (2007). Stabilizing greenhouse gas concentrations at low levels: An assessment of reduction strategies and costs. Climatic Change, **81,** 119–159.

Wang, F., Xu, Y.J., Dean, T.J. (2011). Projecting Climate Change Effects on Forest Net Primary Productivity in Subtropical Louisiana, USA. Ambio **40,** 506–520.

Wang, L., Gong, W., Ma, Y. and Zhang, M. (2013). Modeling regional vegetation NPP variations and their relationships with climatic parameters in Wuhan, China. Earth Interact., 17, 1–20.

WorldClim, (2013). Climate Layers. Available at http://www.worldclim.org/ Accessed 12 June 2014.

Yilmaz, K.T. (1998). Ecological diversity of the eastern Mediterranean region of Turkey and its conservation. Biodivers. Conserv., **7,** 87–9